

# Unipolar Time-Differential Pulse Response with a Solid-State Charpak Photoconductor

A. H. Goldan<sup>a,1</sup>, O. Tousignant<sup>b</sup>, K. S. Karim<sup>c</sup>, J. A. Rowlands<sup>d</sup>

<sup>a</sup> *Department of Radiology, School of Medicine, SUNY at Stony Brook, NY, US*

<sup>b</sup> *ANRAD Corporation, 4950 Levy Street, Saint-Laurent, PQ, Canada*

<sup>c</sup> *Electrical and Computer Engineering, University of Waterloo, Waterloo, ON, Canada*

<sup>d</sup> *Thunder Bay Regional Research Institute, Thunder Bay, ON, Canada*

## ABSTRACT

1

2 We demonstrate a high granularity multi-well solid-state detector with the  
3 unipolar time-differential property. Results show an improvement in the tem-  
4 poral pulse response by more than two orders-of-magnitude using amorphous  
5 selenium as the photoconductive film. The significance of the results presented  
6 here is the ability to reach the intrinsic physical limit for detector pulse speed by  
7 transitioning from the slow transit-time-limited response which depends on the  
8 bulk carrier transport mechanism, to the ultrafast dispersion-limited response  
9 which depends on the spatial spreading of the collected carrier packet.

---

<sup>1</sup>E-mail: Amirhossein.Goldan@stonybrookmedicine.edu

10     Soon after the Nobel prize winning invention of the gas-filled multiwire proportional cham-  
 11 ber (MWPC) by Charpak<sup>[1]</sup>, and parallel to developments in microelectronics, a great deal  
 12 of research was stimulated to develop the highest *granularity*<sup>[2]</sup> gaseous detectors for achiev-  
 13 ing the highest position resolution. However, the practical benefits of high granularity was  
 14 restricted by the micro- to milli-metre range of the radiation induced photoelectron cloud  
 15 in gas. Solid materials, on the other hand, can have three orders-of-magnitude shorter pho-  
 16 toelectron range due to much higher density, and thus, they yield much smaller detector  
 17 dimensions with substantially higher spatial and temporal resolution<sup>[3]</sup>. The problem is that  
 18 disordered solids, which are easier and less expensive to develop than single crystalline solids,  
 19 have been ruled out as viable radiation detection media because of slow pulse response, which  
 20 is attributed to their low carrier mobilities and transit-time-limited photoresponse.

21     In this letter, we show a high granularity multi-well solid-state detector (MWSD) fab-  
 22 ricated using photolithography and film evaporation techniques<sup>[4]</sup>. We directly probe the  
 23 transit of photoinduced carriers in the MWSD using time-of-flight (TOF) transient photo-  
 24 conductivity measurements and show time-differential responses to optical laser and x-ray  
 25 excitations.

26     Let's consider a medium within which a single drifting excess carrier is contained. Ac-  
 27 cording to the Ramo-Shockley theorem<sup>[5]</sup>, the induced current on the collector due to carrier  
 28 displacement inside the medium is given as

$$I_i(t) = q \frac{\partial V_W}{\partial t} = q\mu F \frac{\partial V_W}{\partial z} \quad (1)$$

29 where  $q$  is the charge of the moving carrier,  $\mu$  is the effective carrier mobility inside the  
 30 medium,  $F$  is the applied external field,  $V_W$  is the *weighting potential*<sup>[6]</sup>, and  $z$  is the carrier  
 31 displacement during time  $t$  which is  $z = \mu Ft$ . Note that the conceptual  $V_W$  is dimension-  
 32 less and is the potential that would exist in the detector with the corresponding collecting  
 33 electrode raised to unity and all other electrodes grounded.

34 Conventionally, a planar photoconductive material is fitted between two parallel contacts  
 35 to form a sandwich cell: one is the drift electrode that is kept at a certain potential,  $V_D$ , with  
 36 proper polarity and magnitude, and the second is the collecting electrode (or the collector)  
 37 that is generally biased at zero potential and connects to the readout electronics for signal  
 38 capture. The weighting potential for these parallel plate detectors (PPDs) is zero at the  
 39 drift electrode and rises linearly to one at the collector (dashed line in Fig. 1). According  
 40 to Eq. 1, such distribution means that the collector is sensitive to real-time bulk transport,  
 41 and thus, pulse response is limited by the carrier transit-time,  $t_T$ , across the photoconductor  
 42 thickness,  $L$  (top inset plot in Fig. 1)

$$I_{i1}(t) = \frac{q}{t_T}(H(t) - H(t - t_T)) \quad (2)$$

43 where  $H(t)$  is the Heaviside step function and  $t_T = L/\mu F$  for an excess carrier drifting across  
 44 the detector thickness. Equation 2, with its well-defined plateau, assumes: (a) medium  
 45 homogeneity, (b) coherent carrier drift with non-dispersive Gaussian transport properties,  
 46 (c) homogeneous field distribution, (d)  $RC \ll t_T \ll \tau_D$ , and (e)  $t_T \ll \tau_{rel}$ , where  $RC$  is the  
 47 time constant of the readout circuit,  $\tau_D$  is the deep-trapping lifetime, and  $\tau_{rel}$  is the dielectric  
 48 relaxation time.

49 Now consider a new device with its weighting potential at zero everywhere in the bulk  
 50 except for a very small region near the collector where it rises sharply to one (solid line in  
 51 Fig. 1). In this case, the induced photocurrent due to a single carrier drift is an impulse  
 52 (bottom inset plot in Fig. 1)

$$I_{i2}(t) = q\delta(t - t_T) \propto \left. \frac{d}{dt} I_{i1}(t) \right|_{t=t_T} \quad (3)$$

53 where  $\delta(t)$  is the impulse function. In this case, the collector is completely insensitive to bulk  
 54 event times of the drifting excess carrier and photoresponse is independent of photoconduc-  
 55 tor material (whether single crystalline or disordered, organic or inorganic) and its carrier

56 transport mechanism (whether coherent or incoherent drift via band transport, multiple-  
57 trapping, or hopping). Note that the shape of  $I_{i2}$  is the time-derivative of  $I_{i1}$  at  $t_T$  and that  
58 rise time at the collector is only limited by the  $RC$  time constant of the readout electronics.

59 To circumvent the problems that originate from poor bulk transport properties in disor-  
60 dered solids, one must use the proposed device with its modified  $V_W$  distribution by decou-  
61 pling the radiation absorbing photoconductor from the collector. In bipolar solids such as  
62 chalcogenide glass amorphous selenium (a-Se), where charge induction is due to the drift  
63 of both electrons ( $-$ ) and holes ( $+$ ) in a conventional PPD, this decoupling has the added  
64 advantage of sensing only the carrier type with a higher mobility-lifetime product (i.e., the  
65 primary carrier) and providing insensitivity of the collector to the transport properties of  
66 the slower carrier type. Such localized preferential sensing of primary carriers, which is also  
67 referred to as unipolar (or single-polarity) charge sensing, can be implemented by (1) proper  
68 potential biasing of the sandwich electrodes to drift primary carriers towards the collector,  
69 and (2) establishing a strong *near-field effect* in the immediate vicinity of the collector using  
70 an *electrostatic shield*. The near-field effect can be established with either a direct approach  
71 using the Frisch grid design<sup>[7,8]</sup> or the small-pixel effect<sup>[6]</sup>, or an indirect approach using the  
72 coplanar pixel electrodes<sup>[9]</sup>.

73 Inspired by Charpak’s MWPC<sup>[1]</sup> and its micropattern variants<sup>[7,8]</sup>, we have fabricated a  
74 solid-state detector with an internal electrostatic shield using grid-on-insulator (GOI) and  
75 a-Se film evaporation techniques<sup>[4]</sup>. The proposed device is called the multi-well solid-state  
76 detector (MWSD) and its structure is shown with schematic in Fig. 2a and with scanning  
77 electron microscope (SEM) cross-section in Fig. 2b. The device consists of an evenly spaced  
78 insulating pillars over the collector with pillars’ top side coated with a conductive layer  
79 to form the shielding grid. Note that for simplicity of fabrication, the insulator over the  
80 collector is not etched, which inhibits neutralization of the drifting charge by the collector.  
81 However, we have limited the build-up of this surface space charge using low-level excitation  
82 for a rested specimen, and thus, space charge perturbation is minimized.

83 The weighting potential distribution of the fabricated device is simulated in Fig. 2c which  
 84 shows a very small change in  $V_W$  in the region between the drift electrode and the grid  
 85 (i.e., the interaction region). However,  $V_W$  changes substantially inside each well in the  
 86 region between the grid and the collector (i.e., the detection region). Similar to the Frisch  
 87 gas chambers<sup>[7,8]</sup> and the coplanar detectors<sup>[9]</sup>, we must bend the electric field lines in the  
 88 drift volume close to the grid so that all primary carriers are steered away from the grid  
 89 and channeled inside the well towards the collector. Thus, we define the field bending ratio  
 90  $r = V_G/V_D$ , where  $V_G$  is the grid bias. For comparison purposes, a conventional PPD without  
 91 the shielding grid was also fabricated on the same substrate and Fig. 2c shows its linear  $V_W$   
 92 distribution.

93 We used the time-of-flight (TOF) transient photoconductivity measurements<sup>[10,11,12,13]</sup> to  
 94 verify our theoretical time-differential prediction in Eq. 3. For all the TOF experiments  
 95 reported in this paper, we operated the devices at room temperature with a bulk field of  
 96  $F = 2 \text{ V}/\mu\text{m}$  and  $r = 0.2$  (i.e., for PPD:  $V_D = 400 \text{ V}$ , for MWSD:  $V_D = 500$  and  $V_G = 100$   
 97  $\text{V}$ ). Also, we considered more realistic experimental impulse-like excitations, in contrast to a  
 98 single drifting excess carrier, where (1) a sheet of carriers is photoinduced close to the drift  
 99 electrode with a blue laser pulse and (2) Gaussian carrier clouds are generated uniformly  
 100 across the bulk with a high energy x-ray pulse. Emphasis is on measured results obtained  
 101 from chalcogenide glass a-Se but conclusions drawn can be extended to other non-dispersive  
 102 inorganic and organic photoconductive materials because of the universal feature of charge  
 103 transport that is independent of their atomic, molecular, and crystalline structures. For  
 104 example, in the case of non-dispersive Markoffian transport, Scher-Montroll (SM) *univer-*  
 105 *sality* of the photocurrent is not applicable and the propagating carrier packet experiences  
 106 spreading which is described by Gaussian statistics<sup>[14]</sup>, where the position of the peak of  
 107 carrier distribution coincides with its spatial mean (Fig. 3a). This spreading is mainly due  
 108 to fluctuations of the shallow-trap release time and, in the small-signal case<sup>[15]</sup>, we can ne-  
 109 glect spreading due to mutual Coulomb repulsion of the free charge density. The Gaussian

110 statistics for the root-mean-square (rms) drift spread,  $\sigma_D$ , and the mean carrier displace-  
111 ment,  $\ell$ , obey time dependencies  $\sigma_D \propto t^{1/2}$  and  $\ell \propto t$ , which yield the well-known relation  
112  $\sigma_D/\ell \propto t^{-1/2}$  (Ref.<sup>[14]</sup>).

113 For optical TOF experiments, we used a VSL337 dye laser tuned to 337 nm wavelength  
114 (for strong absorption in a-Se) and 5 ns pulse duration (for impulse-like excitation). Figure  
115 3b shows non-dispersive hole photocurrent transients in a-Se. The result obtained from  
116 the PPD shows a semi-rectangular pulse with a soft plateau, due to inhomogeneous field  
117 distribution, followed by an exponential decay which is the Gaussian integral of the total  
118 drift spread. However, the MWSD response shows a Gaussian pulse (centered at the hole  
119 transit time  $t_{T+}$ ) that verifies the time-differential property of Eq. 3. The time-differential  
120 Gaussian TOF, which is similar to a typical time distribution of Charpak's MWPC (Fig.  
121 29 in Ref.<sup>[16]</sup>), signifies the ability to reach the intrinsic physical limit for pulse speed in  
122 non-dispersive solids.

123 For high energy penetrating radiation, photon interaction can occur throughout the bulk  
124 which results in depth-dependent signal waveform variations in PPDs<sup>[6]</sup>. However, sig-  
125 nal waveforms are depth-independent and unipolar in the MWSD because only holes drift  
126 through the multi-well and are sensed by the collector. Thus, the detector pulse speed is  
127 improved substantially by a factor of  $n \leq (L/4\sigma)(\mu_+/\mu_-)$ , where the first term is due to  
128 the time-differential property, the second term is due to the unipolarity,  $\sigma$  is the total rms  
129 spread, and  $4\sigma$  is approximately the Gaussian pulse width. As shown in Fig. 3c,  $n$  is equal  
130 to  $\sim 300$  for a-Se comparing hole-dispersion-limited response with that of electron-transit-  
131 time-limited.

132 The next experiment extends the concept of optical TOF to x-rays that is also applicable  
133 to a blocking drift electrode<sup>[13]</sup>. The x-ray TOF is different from optical TOF in that (1)  
134 photon absorption can occur throughout the photoconductor, and (2) a Gaussian charge-  
135 cloud is formed around the primary interaction site of each absorbed photon (inset of Fig.  
136 4). The rms spreading  $\sigma_R$  of the charge cloud (i.e., the photoelectron range) obeys the

137 relation  $\sigma_R \propto E^2$  in a-Se<sup>[17]</sup>, where  $E$  is the energy of the absorbed x-ray photon. For x-  
 138 ray excitations, we used an XR200 pulsed source tuned to 150 kvP (for a nearly uniform  
 139 charge-cloud generation density across the photoconductor thickness), 3 mR exposure (for  
 140 maintaining the small-signal case), and 60 ns pulse duration (for impulse-like excitation).  
 141 The measured time-resolved transients in Fig. 4 show a linear decay (i.e., triangular response)  
 142 for the conventional PPD due to carrier neutralization at the collector (or in our case, carrier  
 143 immobilization at the Se-PI interface), and a nearly constant response (i.e., rectangular) for  
 144 the proposed MWSD, verifying once again the time-differential property. An important  
 145 feature of the x-ray time-differential response is the observed exponential tail, representing  
 146 the actual Gaussian distribution of the last drifting hole packet that was initially generated  
 147 close to the drift electrode from an absorbed x-ray photon with  $E = 60$  keV. This response  
 148 at the tail shows the physical limit for the photoconductor's temporal performance due to  
 149 the total spatial spreading  $\sigma = \sqrt{\sigma_D^2 + \sigma_R^2} = 0.07$ . Note that the spike observed at the  
 150 onset of the x-ray pulse is the result of surface space-charge perturbation. The magnitude  
 151 of this spike is larger for the MWSD because of its higher field in the detection region (Fig.  
 152 4 with the top-right axes).

153 An important non-ohmic effect in disordered solids may occur in the presence of a strong  
 154 field with the transport mechanism shifted from localized states into extended states where  
 155 the mobility can be 100 to 1000 times higher<sup>[18]</sup>. Such hot carriers in extended states (with  
 156 mobilities near the mobility edge) can gain energy faster than they lose it to phonons, and  
 157 thus, avalanche due to impact ionization is possible (e.g., hot holes in a-Se<sup>[19]</sup> in contrast to  
 158 hot electrons in amorphous silicon<sup>[20]</sup>). Continuous and stable avalanche multiplication has  
 159 been shown in a-Se, a feature that enabled the development of an optical camera with more  
 160 sensitivity than the human eye (i.e., 11 lx at aperture F8, or 100 times more sensitive than  
 161 a CCD camera)<sup>[21]</sup>. For high-energy penetrating radiation, the challenge is that avalanche-  
 162 mode selenium cannot be the bulk medium because (1) avalanche layers cannot be very  
 163 thick ( $< 25\mu\text{m}$ ) and (2) a uniform avalanche field in the bulk causes depth-dependent gain  
 164 variations. Our proposed MWSD (Fig. 2b) is the practical approach for achieving stable

165 avalanche in large-area direct radiation detectors, where the low-field interaction region can  
166 be made as thick as necessary to stop high-energy radiation, and the high-field multi-well  
167 detection region can be optimized for avalanche multiplication.

168 In conclusion, we have designed, fabricated, and characterized a high granularity multi-  
169 well solid-state detector which achieves ultrafast unipolar time-differential pulse response.  
170 It is important to remark that we were able to reach the physical limit of pulse speed in  
171 a-Se set by the spatial spreading of the collected hole cloud. Future studies are envisaged  
172 to build devices with proper blocking contacts for achieving avalanche-multiplication gain in  
173 the wells, with applications ranging from high-energy and nuclear physics to industrial and  
174 medical diagnostics and crystallography<sup>[22,23]</sup>. Furthermore, advances in nano-electronics can  
175 be applied to manufacture the highest granularity nanopattern solid-state detectors (NSSD)  
176 with ultrafast time-differential photoresponse, due to the nanoscale photoelectron range in  
177 solids in response to impulse excitations in a continuum from the visible to the soft x-rays,  
178 with applications in optical communications<sup>[24]</sup> and time-domain spectroscopy<sup>[25]</sup>.

179

#### ACKNOWLEDGEMENTS

180 We are grateful to Dr. Giovanni DeCrescenzo for help with the characterization of the  
181 detectors. Multi-well structures were fabricated photolithographically using the Giga-to-  
182 Nanoelectronics Centre facilities at the University of Waterloo and amorphous selenium  
183 films were deposited at ANRAD corporation.

184

#### FIGURE CAPTIONS

185 **Figure 1:** Weighting potential distributions for a conventional PPD (dashed line) and a  
186 new hypothetical detector (solid line). Insets show the corresponding induced photocurrents  
187 due to a single excess carrier drift.

188 **Figure 2:** (A) Schematic diagram for our realization of the proposed device, called  
189 the multi-well solid-state detector (MWSD). (B) SEM cross-sections of the representative  
190 device. The polyimide (PI) pillars are  $11.5 \mu\text{m}$  in height and are evenly distributed over



191 the chromium (Cr) collector with a pitch of  $10\ \mu\text{m}$ . Their top surface is covered with Cr  
 192 to form the shielding grid electrode. To ensure blocking contacts for limiting the excess  
 193 charge injection, the grid is coated with another thin PI layer. A  $200\ \mu\text{m}$  a-Se film is  
 194 evaporated over the structure as the photoconductive material (i.e.,  $L = 200\ \mu\text{m}$ ), and  
 195 finally, a semi-transparent gold (Au) layer is sputtered on top to provide the drift electrode  
 196 while enabling optical excitation measurements. The top contact is non-blocking not to  
 197 impede the extraction of optically induced carriers. **(C)** Weighting potential distributions for  
 198 carriers terminating on the collector and on the grid.

199 **Figure 3:** **(A)** Schematic representation of carrier packet transport optically induced  
 200 close to the drift electrode in a non-dispersive solid. **(B)** Hole TOF transients in a-Se PPD  
 201 and MWSD structures. Gaussian TOF transient in the MWSD with  $(\sigma_D/\ell)_{t_{T+}}=0.04$ , shows  
 202 the time-differential property. **(C)** Logarithmic TOF plots showing the signal pulse widths.  
 203 For an x-ray photon absorbed close to the collector, holes are immediately neutralized and  
 204 only electrons are in motion towards the drift electrode. Thus, pulse speed is limited by  
 205 the electron transit time  $t_{T-}$  in a-Se PPDs, as shown from the measured electron TOF.  
 206 Measured a-Se effective electron and hole mobilities are  $\mu_- = 0.002$  and  $\mu_+ = 0.1\ \text{cm}^2\ \text{V}^{-1}$   
 207  $\text{s}^{-1}$ , respectively.

208 **Figure 4:** Bottom-left axis: Linear-decay x-ray TOF response of the PPD and unipolar  
 209 rectangular response of the MWSD, showing once again its time-differential pulse response.  
 210 The measured total spreading of the Gaussian tail is  $(\sigma/\ell)_{t_{T+}}=0.07$ . Top-right axis: Elec-  
 211 tric field distribution in the bulk. Top inset shows schematic representation of Gaussian  
 212 photoelectron clouds created at the onset of radiation ionization.

## REFERENCES

- [1] G. Charpak, Nature **270**, 479 (1977).
- [2] Granularity is the distance between the anode and the cathode electrodes in the detection region.
- [3] G. Charpak and F. Sauli, Ann. Rev. Nucl. Part. Sci. **34**, 285 (1984).

- [4] A. H. Goldan and K. S. Karim, U.S. Patent No. 8,129,688 B2 (2012).
- [5] L.Y. Chen and C.S. Ting, Phys. Rev. Lett. **64**, 3159 (1990).
- [6] H. H. Barrett, J. D. Eskin, and H. B. Barber, Phys. Rev. Lett. **75**, 156 (1995).
- [7] Y. Giomataris, Nucl. Instr. and Meth. A **376**, 29 (1996).
- [8] F. Bartol, M. Bordessoule, G. Chaplier, M. Lemonnier, and S. Megtert, J. Phys. III (France) **6**, 337 (1996).
- [9] P. N. Luke, Appl. Phys. Lett. **65**, 2884 (1994).
- [10] W. Spear, Journal of Non-Crystalline Solids **1**, 197 (1969).
- [11] G. Juška, K. Arlauskas, and M. Viliunas, and J. Kočka, Phys. Rev. Lett. **84**, 4946 (2000).
- [12] A. Pivrikas, G. Juška, A. J. Mozer, M. Scharber, K. Arlauskas, N. S. Sariciftci, H. Stubb, and R. Österbacka, Phys. Rev. Lett. **94**, 176806 (2005).
- [13] A. W. Rau, L. Bakueva, and J. A. Rowlands, Med. Phys. **32**, 3160 (2005).
- [14] H. Scher and E. Montroll, Phys. Rev. B **12**, 2455 (1975).
- [15] A. Many and G. Rakavy, Phys. Rev. **126**, 1980 (1962).
- [16] G. Charpak, Ann. Rev. Nucl. Sci. **20**, 195 (1970).
- [17] W. Que and J. A. Rowlands, Med. Phys. **22**, 365 (1995).
- [18] N. F. Mott, Phil. Mag. **24**, 935 (1971).
- [19] G. Juška and K. Arlauskas, Phys. Status Solidi A **59**, 389 (1980).
- [20] G. Juška, K. Arlauskas, J. Kočka, M. Hoheisel, and P. Chabloz, Phys. Rev. Lett. **75**, 2984 (1995).
- [21] K. Tanioka, J. Mater. Sci.: Mater. Electron. **18**, 321 (2007).
- [22] F. S. Goulding and Y. Stone, Science **170**, 280 (1970).
- [23] J. Miao, P. Charalambous, J. Kirz, and D. Sayre, Nature **400**, 342 (1999).
- [24] T. Mueller, F. Xia, and P. Avouris, Nature Photonics **4**, 297 (2010).
- [25] B. Ferguson and X. Zhang, Nature Materials **1**, 26 (2002).

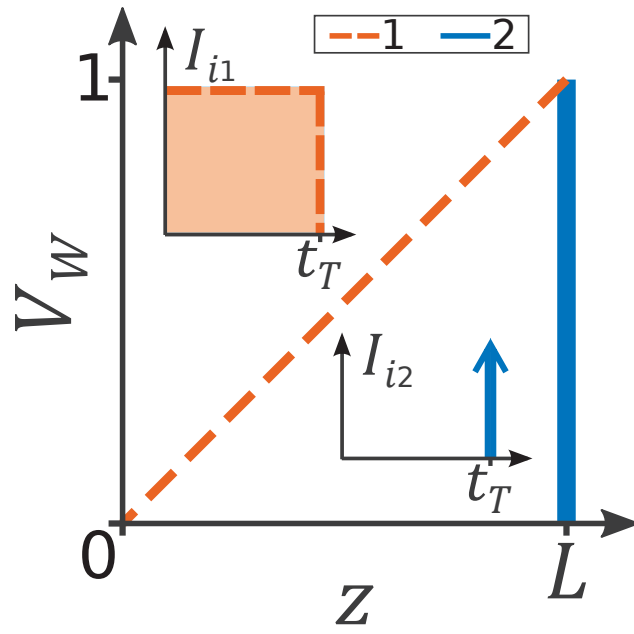
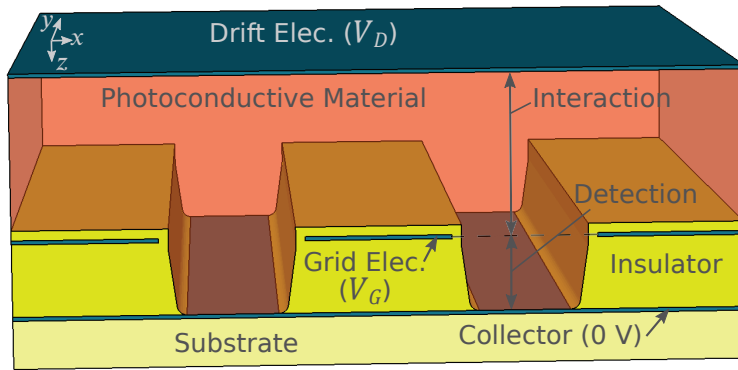
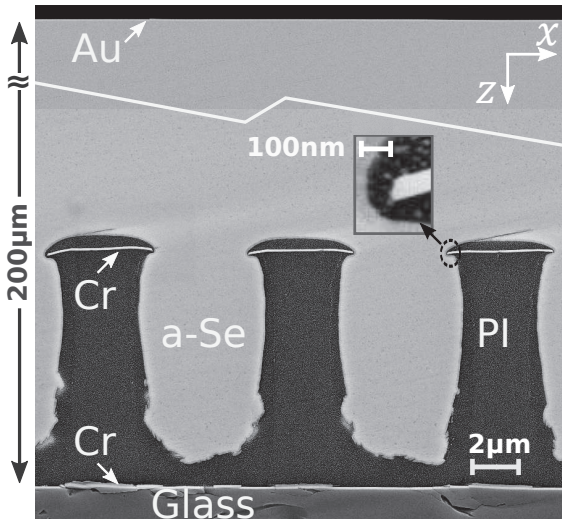


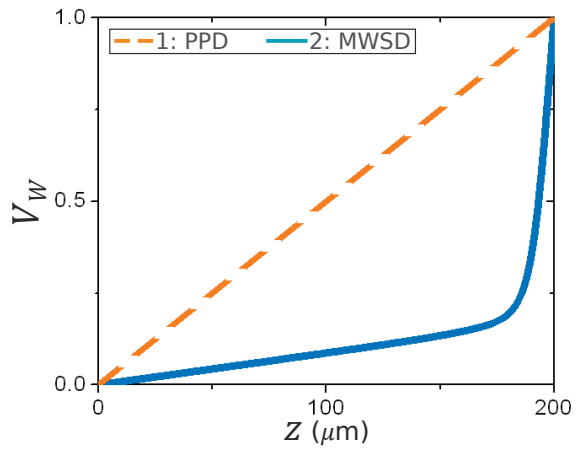
FIGURE 1



(A)



(B)



(c)

FIGURE 2

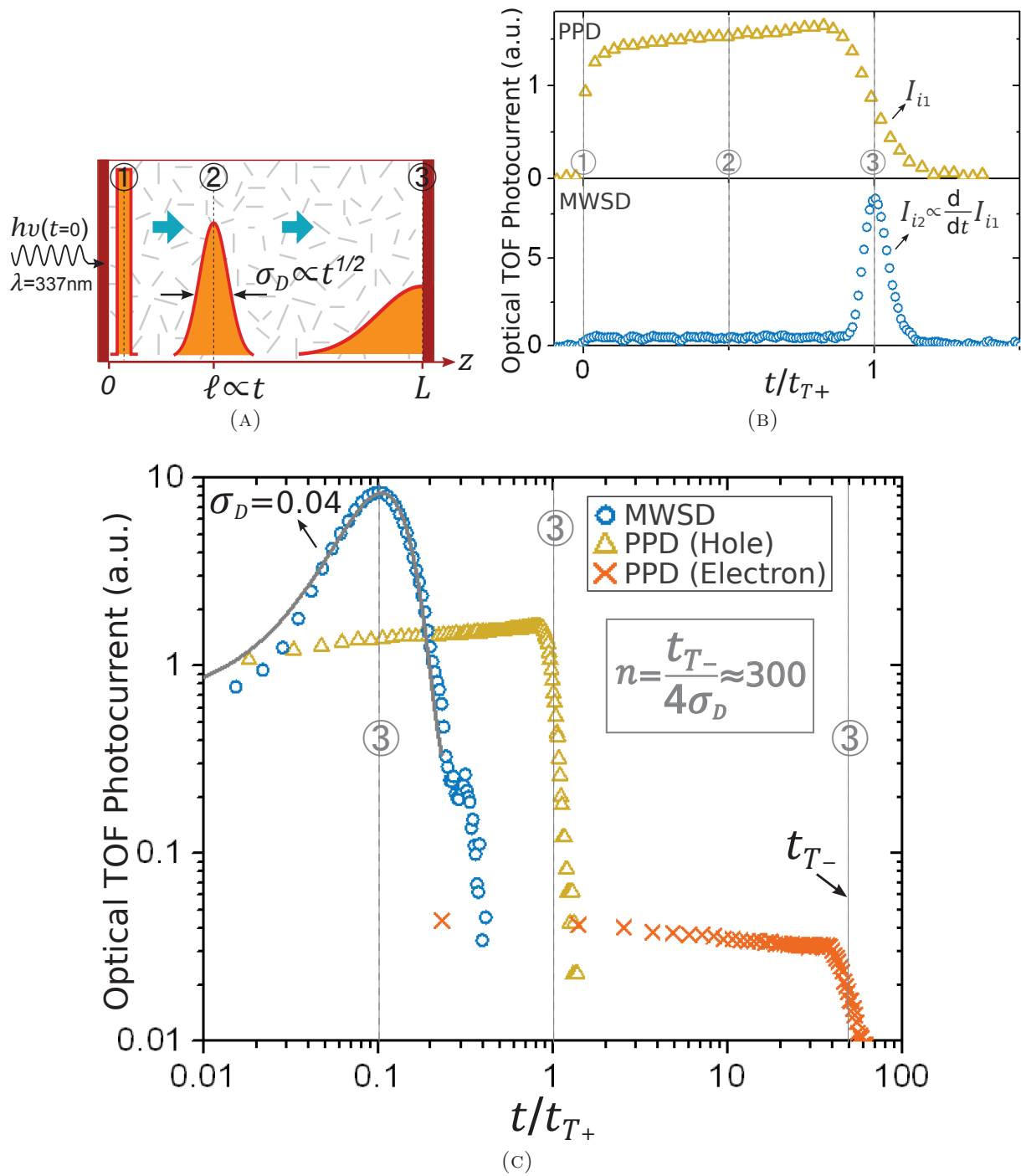


FIGURE 3

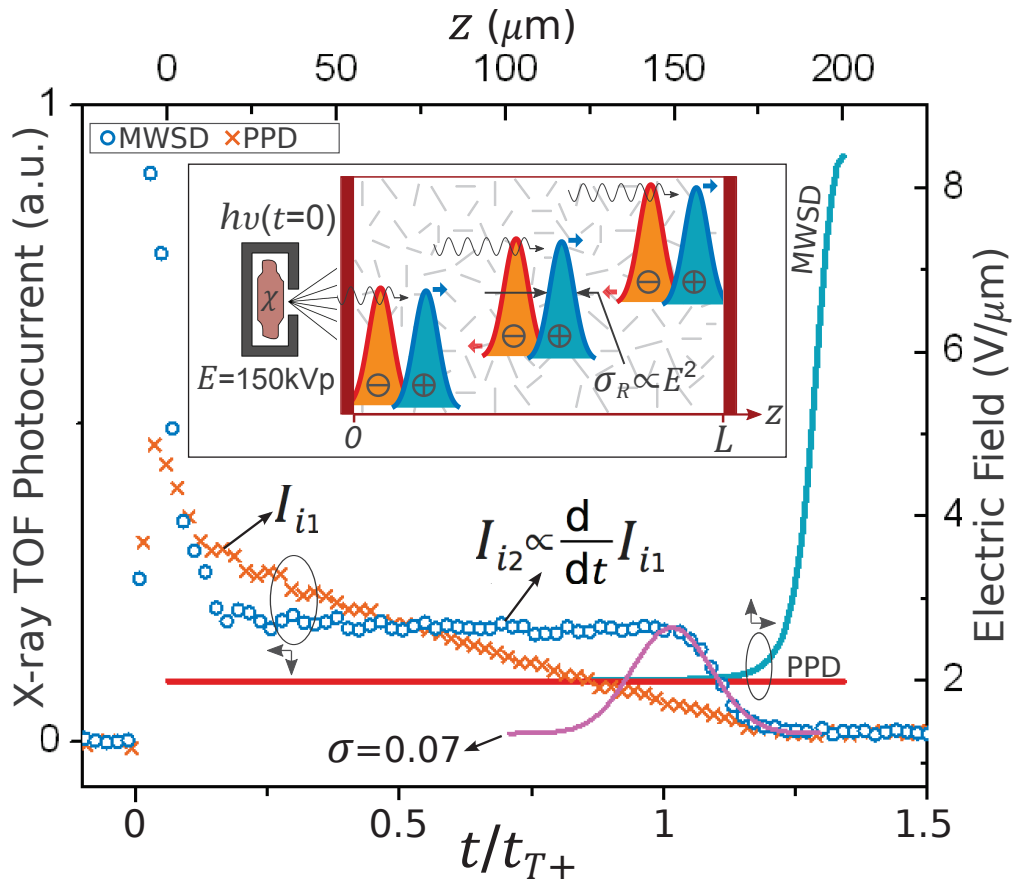


FIGURE 4